LIMNOLOGY and OCEANOGRAPHY

ASLO

Limnol. Oceanogr. 9999, 2021, 1–15

doi: 10.1002/lno.11764

Whole-lake methane emissions from two temperate shallow lakes with fluctuating water levels: Relevance of spatiotemporal patterns

Marcel Schmiedeskamp,[1*] **Leandra Stephanie Emilia Praetzel**,[1] **David Bastviken**,[2] **Klaus-Holger Knorr**[1*]

[1]Ecohydrology and Biogeochemistry Group, Institute of Landscape Ecology, University of Münster, Münster, Germany
[2]Department of Thematic Studies—Environmental Change, Linköping University, Linköping, Sweden

Abstract

Globally, shallow lakes are an important source of methane (CH_4) emissions to the atmosphere. Previous studies of such lakes have rarely focused on the within-lake spatiotemporal variability, which is critical for generating representative whole-lake fluxes, and better understanding and constrain large-scale emissions. To address this issue, we determined the variability of CH_4 fluxes and CH_4 concentrations in two small shallow (≤ 150 cm) lakes in Central Europe biweekly over almost 2 years. We found that both lakes were a source of CH_4, mainly by ebullition. At the shallower Lake Heideweiher, which temporarily dried out, the average flux was 7.2 mmol m^{-2} d^{-1}, the average flux from Lake Windsborn that never dried out, was 3.5 mmol m^{-2} d^{-1}. The spatial differences (between and within lakes) were most strongly related to sediment C-content and quality, which in turn was linked to depth or distance to shore. The highest fluxes occurred in the central parts of both lakes. The temporal variability of the fluxes was primarily correlated with sediment temperature and degree of drying measured as the time since drying up. The whole-lake estimates were dominated by low water periods and the warm summer months. Overall, we show that short-term and small-scale measurements cannot account for the high variability of CH_4 fluxes from small lakes, and that reliable large-scale assessments need to consider such spatiotemporal variability.

Methane (CH_4) is currently the second most important greenhouse gas. In 2011, concentrations of CH_4 exceeded preindustrial levels by about 150% (IPCC 2013; Saunois et al. 2020). Although inland waters cover only a small fraction of the earth's surface, they are globally important sources of CH_4 (Tranvik et al. 2009; Bastviken et al. 2011). Lakes are estimated to contribute 9–24% to total annual CH_4 emissions (Saunois et al. 2020), representing the second largest natural source after wetlands; small shallow lakes have been suggested to be particularly important (Tranvik et al. 2009; Downing 2010; Holgerson and Raymond 2016).

Over 90% of all lakes are smaller than 0.01 km^2 (Downing 2010; Verpoorter et al. 2014). Due to their small area and, thus, closer distance to the shore and the greater shore to volume ratio, more organic carbon transported from the catchment into these lakes can fuel CH_4 formation in the anaerobic sediments. Morevover, there may be considerable benthic or water column primary production in shallow lakes because almost the entire water column is penetrated by light, providing additional organic matter to the sediments.

Even though shallow lakes are large CH_4 emitters, still little is known about the temporal and spatial dynamics of CH_4 fluxes in shallow lakes across different ecoclimatic regions. Numerous studies have been addressing spatial variability over short measurement periods, but apparently only a handful papers, primarily from subarctic, boreal, and subtropical regions, systematically addressed temporal variability with frequent samplings over full years (e.g., Natchimuthu et al. 2016; Jansen et al. 2019; Jeffrey et al. 2019). Among these few studies, temperate ecoregions seem underrepresented.

CH_4 fluxes can be highly variable and have different emission pathways, including diffusion, ebullition, or transport via plant aerenchyma (Bastviken et al. 2004). In particular, shore areas are considered to be "hot spots" of high CH_4 concentrations because of reduced oxidation of CH_4 in the shallow water column, low hydrostatic pressure, and consequently larger pressure variation from, for example, waves on the sediments, facilitating bubble release (Bastviken et al. 2004; Kankaala et al. 2013; Holgerson and

*Correspondence: m.schmiedeskamp@uni-muenster.de; kh.knorr@uni-muenster.de

Additional Supporting Information may be found in the online version of this article.

Raymond 2016). Hence, the whole areas of shallow lakes could sustain high fluxes.

The dominant pathway for the total CH_4 flux is usually episodic ebullition, which can account for 50% to > 90% of the total CH_4 emissions (Casper et al. 2000; Bastviken et al. 2004; Natchimuthu et al. 2016). Suggested predictors for CH_4 flux through ebullition include temperature and pressure (Mattson and Likens 1990), and the properties of the sediment organic material with input of recently produced organic matter of low C : N ratio suggested to be favorable for CH_4 formation (Duc et al. 2010; Wik et al. 2018).

We studied CH_4 emissions from the open-water areas of two temperate lakes in Central Europe. Our aim was to provide a comprehensive assessment of open water lake CH_4 fluxes and flux regulation in both space and time. We used floating chambers and performed measurements over a period of 2 years during the ice-free season to analyze CH_4 emissions, surface water CH_4 concentrations and potential drivers, such as temperature, stratification, oxygen content of the water column, wind, water depth, sediment organic carbon content, and sediment C : N ratio. One of the two lakes partially temporarily dried out during the summer months; thus, we estimated the effect of drying on fluxes.

We hypothesized that (1) CH_4 flux and concentration would follow a temporal pattern along the seasonal temperature amplitude and would be highest during summer months; (2) CH_4 flux and concentration vary spatially and would be highest in areas with low water depths and higher input of organic matter to sediments.

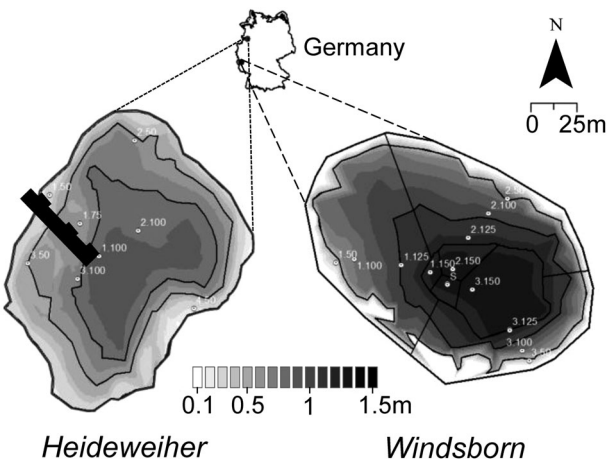

Fig. 1. The study lakes Heideweiher (left) and Windsborn (right) in the west of Germany. Marked positions in the lakes are chamber positions (white circles) representing all water depth categories. Lake Heideweiher was measured along four transects (1, 2, 3, 4—thin solid black line) and along two depth categories (50, 100). In 2018 we constructed the boardwalk (solid thicker black line, not to scale) and added site 75. Lake Windsborn was measured along three transects (1, 2, 3—thin solid black line) and along four depth categories (50, 100, 125, 150).

Material and methods

Study sites

The lakes studied were the two polymictic lakes Windsborn (WB; a crater lake located in the nature conservation area Reihenkrater Mosenberg und Horngraben in the Eifel District, Western Germany), and Lake Heideweiher (HW; in the nature conservation area Heiliges Meer in the Northwest of Germany). The area of Lake Windsborn is ~15,800 m^2 with a maximum depth between 120 and 170 cm depending on the water level. It is located at 480-m elevation and surrounded by pyroclastic crater walls of about 20 m in height less than 80 m away from the shore (Praetzel et al. 2020). Thus, the lake has a catchment of only 8 ha, no surface inflow and, therefore, is primarily fed by precipitation and only insignificant contributions of groundwater. The lake is nearly devoid of macrophytes and surrounded by deciduous trees. The Lake Heideweiher has a similar area of 15,470 m^2 but is shallower with a maximum depth of 83 cm and extreme seasonal water fluctuations, concomitant drying up of the shore areas, and possibly complete drying up of the lake in above-average warm and dry summers. It is fed by shallow groundwater and by rainwater, depending on the groundwater level. The sediment consists of Weichsel glacial period sands and drifted deck sands interspersed with embedded peat. At about 40 cm sediment depth there is an iron rich hardpan, which inhibits the infiltration of rainwater (Weinert et al. 2000). At low groundwater levels, the lake drains to the aquifer. At high levels, groundwater influence occurs. Due to the shallow depth, a large part of the water body is covered with emergent macrophytes, primarily *Nymphaea alba* (L.), from April until the end of the vegetation period in October. The lake is surrounded by a mixture of agricultural land use, heathland, grassland, and partly forested area. To access the lake, a boardwalk was constructed at transect 1 (Figs. 1, S1). Both lakes were intermittently covered with ice between December and March.

Lake Windsborn was sampled biweekly during the ice-free season from April to November 2017 and March to November 2018. Lake Heideweiher was visited biweekly from March to August 2017 and March to November 2018. In total, we realized 34 and 28 measurement campaigns at Lake Windsborn and Lake Heideweiher, respectively. In Lake Windsborn, we measured along three spatial transects from shore to center, separated in depth categories of the water column up to ~ 50 (< 50 cm), ~ 100 (50 to < 100 cm), ~ 125 (100 to < 125 cm), and ~ 150 cm (125–150 cm) to cover the spatial variability (Natchimuthu et al. 2016). One additional site "S" was placed at the intersection of the three transects in the center of the lake in depth category 150 to represent the maximum distance from the shoreline (Fig. 1). At Lake Heideweiher, we used the same depth categories but due to the shallower lake depth, there were only categories ~ 50 and ~ 100 cm in 2017. In contrast, in 2018, we performed measurements along a single

Table 1. Mean, range (min–max), and number of observations of surface water and sediment parameters of the lakes. Cont. means continuous measurement.

	Windsborn		Heideweiher	
	n	Mean (range)	*n*	Mean (range)
Area (ha)	Cont.	1.4 (1.3–1.6)	Cont.	0.9 (0–1.5)
Water level (cm)	Cont.	124 (100–151)	Cont.	40 (0–83)
Annual precipitation (mm)	2	620 (539–700)	2	511 (450–634)
Water characteristics				
pH	810	6.9 (5.4–9.0)	114	4.6 (4.3–7.4)
Conductivity (μS cm^{-1})	772	19.3 (16.1–22.8)	92	49.1 (38.8–64.7)
O_2 (mg L^{-1})	792	9.7 (5.6–12.1)	84	9.0 (0–11.9)
O_2 (%)	792	110 (66–142.1)	84	99.7 (0–133.4)
Chlorophyll α (μg L^{-1})	806	29.9 (5.4–60.0)	18	41.9 (7.5–403)
DOC (mg L^{-1})	836	13.7 (8.5–21.8)	247	18.1 (0.3–44.1)
Total P (μg L^{-1})	834	60 (10–380)	231	40 (< 10–200)
TDN (mg L^{-1})	830	0.9 (0.4–2.2)	231	1.9 (0.03–5.8)
Total Ca (mg L^{-1})	834	1.1 (0.5–2.3)	231	1.8 (0.6–4.9)
Total Fe (mg L^{-1})	834	0.1 (0.02–0.2)	231	0.2 (0.01–0.4)
Total S (mg L^{-1})	834	0.4 (0.2–2.2)	231	2.4 (1.3–3.0)
Sediment characteristics				
Sediment temperature	Cont.	12 (0.5–24)	Cont.	13 (−0.3 to 26)
C%	12	25.0 (2.2–32.2)	10	29.2 (12.5–43.4)
N%	12	1.9 (0.2–2.5)	10	1.9 (0.7–3.0)
C : N ratio	12	13.8 (11.0–18.4)	10	16 (14.4–20.0)

additional transect along a boardwalk which again included both depth categories but additionally a depth category of ~ 75 cm (50 to < 75 cm) instead of the other transects 2, 3, and 4. During our measurement campaigns in 2017 and 2018, the lakes exhibited high seasonal variability in nutrient and carbon concentrations as shown along with other characteristics in Table 1.

Flux measurement

Flux measurements were performed at each site using floating plastic chambers, based on Gålfalk et al. (2013) (*see* Supporting Information Appendix S1 for description of the chambers). These chambers were set up for 24 h to include daily flux fluctuations. After placing the chamber, an initial air sample was taken through a tubing with a 60-mL plastic syringe. After 24 h, we again sampled air from the headspace inside the chamber, the headspace was mixed by repeated pumping with the syringe prior to sampling. The gas samples were subsequently transferred into 8.5-mL crimp vials, previously closed with black butyl rubber stoppers and flushed with N_2. To transfer the sample, an inflow and an outflow needle were injected through the rubber stopper into the vial. By injecting 55 mL of the sample, the vials were completely flushed with the sample. Subsequently, the remaining 5 mL were injected after the removal of the outflow needle, whereby all samples were stored overpressurized. All samples were analyzed within 24 h.

Due to the lake drying up in 2018, the measurement setup at Lake Heideweiher was modified. Instead of 24-h floating chamber measurements, collar measurements were taken for 3–5 min at the boardwalk for the depth categories of 50, 75, and 100 cm, each with three replicates. The collars—installed 28 cm into the soil—were cylindrical with a diameter of 18.9 cm (0.028 m^2) and a total height of 30 cm. Cylindrical plexiglas chambers covered with reflective insolation foil were used for the flux measurements. CH_4 concentrations were quantified with an Ultraportable Greenhouse Gas Analyzer (915-001, Los Gatos Research Inc., Mountain View, California) at a temporal resolution of 1 Hz.

Flux calculations

The CH_4 fluxes determined by floating chambers were adjusted for nonlinearity using the equation:

$$F(\mathrm{CH_4}) = k \cdot (\mathrm{C_w} - \mathrm{C_{fc}}), \quad (1)$$

where F is the CH_4 flux in mol m^{-2} d^{-1}, k is the piston velocity in m d^{-1}, C_w is the measured CH_4 concentration in the surface water in mol m^{-3}, and C_{fc} is the CH_4 concentration in the water in the equilibrium with chamber headspace (mol m^{-3}). To consider the accumulation of CH_4 in the headspace over the 24-h period,

the k was corrected for the nonlinear increase of CH_4 concentration in the headspace as described in detail by Bastviken et al. (2004). The corrected exchange coefficient k was normalized to a Schmidt number of 600 (k_{600}) (details are in Supporting Information Appendix S1). A larger amount of ebullition increased the calculated k_{600}, so the k value was used to distinguish between diffusive and ebullition flux. Therefore, the k_{600} of each chamber at the actual measurement day was divided by the minimum k_{600} of the same day. Following Bastviken et al. (2004) and Schilder et al. (2013), a ratio of < 2 indicated only diffusive flux. Where k values indicated considerable ebullition, we used the linear approach to determine the total flux. The amount of ebullition flux was the result of subtracting diffusive from total flux.

Total fluxes from the Ultraportable Greenhouse Gas Analyzer (UGGA) were calculated based on the gas concentration change in the floating chamber and sediment chambers over time using linear regression and the ideal gas law, air temperature, and air pressure. For calculation of the diffusive flux of the UGGA measurements, bubble events were ignored and only linear slope segments of $r^2 > 0.9$ and $p < 0.05$ were considered. The proportion of ebullition was found obtained subtracting the diffusive from the total flux.

CH_4 concentrations

Surface water CH_4 concentrations were determined in samples taken near each of the chambers at the start and end of the flux measurement using the headspace method. We collected 2 mL of water with a syringe and transferred the sample into an 8.5-mL crimp vial spiked with 200 μL of 2 M HCl and closed including background air with a rubber stopper and crimp cap.

The dissolved concentration was calculated from gas chromatographic analysis of the headspace, using the ideal gas law for the gas phase and Henry's law adjusted for temperature (Sander 1999) for the solute phase to calculate total amounts of CH_4 in the vial, considering the background air in the vial, and dividing the remaining amount by the initial water volume. In addition, we determined CH_4 concentrations in the water column under the ice through a drilled hole on 02 March 2018, in Lake Windsborn. See Supporting Information (Fig. S7) for CH_4 concentration profiles in the water column and ice cover measurements.

Laboratory analyses

Gases

For the analysis of the dissolved CH_4 concentration, 2 mL of gas was extracted from the vials using a syringe and measured on a gas chromatograph (SRI 8610 equipped with methanizer and flame ionization detector, SRI Instruments, Europe, Germany).

Sediment

Sediment samples were taken at two occasions in May 2017 and February 2018 at all eight sites within Lake Heideweiher. At each site, 60-cm long sediment cores were taken in duplicate using a gravity corer (UWITEC, Mondsee, Austria). For analysis only the upper 0–5 cm were considered. The samples were freeze dried, ground, and analyzed for total carbon (C), nitrogen (N) using isotope-ratio mass spectrometry (Eurovector EA3000 coupled with Nu Instruments Nu Horizon, Hekatech, Wegberg, Germany). Details of the method were described in Praetzel et al. (2020). The proportion of inorganic carbon was less than 0.1% and was therefore neglected. We calculated a molar ratio (C : N ratio) from sediment C and sediment N.

Environmental parameters

During the study period at both lakes, air temperature, water surface temperature (10 cm), deep water temperature (Windsborn 90 cm; Heideweiher: 50 cm), sediment temperature (5–10 cm inside the sediment), relative humidity, pH, air pressure, wind speed at 200 cm, wind direction, photosynthetically active radiation, and precipitation were recorded at central floating platforms by HOBO RX3000 Stations—CELL-3G weather station (RX3003-00-01 [3G], Onset, Bourne, Massachusetts) at a temporal resolution of 10 min.

On each day of measurement, pH, O_2, conductivity, and temperature were measured manually at each location using a handheld probe (WTW Multi 3420 Set G, Weilheim, Germany). The water level was determined by pressure transducers in a 30-min interval (Solinst Levellogger 3001, Solinst Ltd., Georgetown, Canada). From the bathymetric map (Fig. 1), we calculated the difference to the water level at the location of the level logger to estimate the water level at each chamber location.

Furthermore, we calculated on the basis of water temperature, the differences in water density, causing temporary stratification. To this end, we calculated Brunt–Väisälä stability frequencies (N_s) (s^{-1}) between surface water at 10 cm depth and deep water at 90 cm (Windsborn) or at 50 cm (Heideweiher) depth, using Eq. 2:

$$N_s = \sqrt{\frac{g}{\rho_w}\frac{\Delta\rho_w}{\Delta z}} \quad (2)$$

in which N_s is the Brunt–Väisälä stability frequency (s^{-1}), g is the acceleration due to gravity ($m\ s^{-2}$), $\Delta\rho_w$ is the gradient in water density ($kg\ m^{-3}$) based on Chen and Millero (1986), and Δz is the water depth gradient (m). We assumed that a stable stratification was present above N_s of 0.055 s^{-1} which corresponds to a value of 0.25 $kg\ m^{-3}\ m^{-1}$ based on threshold of Huotari et al. (2011) and therefore we are in the middle range of the density-dependent estimates of stratification thresholds from 0.07 to 0.5 $kg\ m^{-3}\ m^{-1}$ reported by Gray et al. (2020). There was no evidence of vertical

gradients in conductivity, and salinity was therefore not included in the calculation of N_s.

Data analysis

All statistical analyses were conducted with R Studio, Version 3.5.2 (R Core Team 2018). Statistical significance was determined at $p < 0.05$ on a 95% confidence interval. Data were tested for normal distribution and homoscedasticity with Shapiro–Wilk and Levene tests. All flux data were gamma distributed, thus significant differences between groups were determined using Kruskal–Wallis and post hoc Dunn tests (Dunn 1964). The temperature flux dependence was described with the Arrhenius equation (Yvon-Durocher et al. 2014)

$$F = A \cdot e^{-\frac{E_A}{RT}} \quad (3)$$

where F is the total flux (mmol m^{-2} d^{-1}), E_A is the empirical activation energy (eV = 96.5 kJ mol^{-1}), T is the temperature (K), R is the gas constant (8.314 J K^{-1} mol^{-1}), and A is the pre-exponential factor. The apparent activation energy was determined via an empirical approach by linear regression of the natural logarithm of the total flux against $1/T$.

Upscaling to the whole-lake estimate

Contour plots of fluxes and concentration data for the whole lake in relation to the distance to shore over the measurement period were created using Surfer 16 (Golden Software, Golden, Colorado) and an inverse distance weighting (IDW) method based on the mean data of the three transects. The resulting interpolation was used for illustrative purposes only and was not used for the upscaling of whole-lake fluxes. Digital maps of the lakes' bathymetry and the investigated sites were created using IDW (ArcGIS 10.7, Esri, Redlands, California). The lakes were divided according to the transects using Thiessen polygons and were subsequently divided into depth segments. We used the determined area proportions of the lake to sum up a whole-lake budget, multiplying the value for a variable at each site with the area proportion of the lake. We weighted the individual flux measurements both in terms of time and their respective depth and area proportion (Fig. 1). To this end, the fluxes from the respective polygons were multiplied by the respective area in m^2 and were linear interpolated until the next measurement time point.

As another approach, we used generalized linear models (GLMs) based on the gamma distribution with a log-link function to determine which environmental variables predicted the total flux of the lakes, and we used the model to get an estimate based on the higher temporal resolution of the environmental data. Models were tested using 24 h means of environmental variables of temperature (air, water, depth water, sediment), wind speed, PAR, water level at site, time since drought ($t_{drought}$; considered as dry when the water level at the chamber of the respective depth category was 0 cm), distance to shore, C-content, C : N ratio, Brunt–Väisälä stability frequencies, rain, pressure. For Lake Heideweiher, the data were separated into fluxes on the open water and fluxes of the dry areas, which were represented by an extra model. Models were fit with all environmental variables and assessed for collinearity by calculating the variation inflation factor (VIF) and removing variables with a VIF ≥ 5. Each maximum model was simplified using Akaike information criterion (AIC) backward. The models were considered adequate when AIC reached the minimum. F tests were used to assess the overall significance of terms in each model. For all models mentioned, we checked the residuals for normality, constant mean, and variance.

Results

CH_4 concentrations in the water column

The surface concentrations of CH_4 in both lakes differed significantly and were 3.9 [0–5.2] ± 1.1 μM (mean [range] ± SD) in Lake Heideweiher and 1.5 [0.1–15.5] ± 1.6 μM in Lake Windsborn. In Lake Heideweiher, CH_4 concentrations strongly increased in spring, especially at the shore sites. As the lake dried out, the concentrations kept increasing in the remaining water until complete drying up in August 2018 (Fig. 2). During low water levels in August 2017 and June/July 2018 at Lake Heideweiher, highest CH_4 concentrations were observed, along with an almost anoxic water column (Fig. 3). In sum, the temporal variability was greater than the spatial variability. Furthermore, no significant effect of the depth category could be determined (Fig. S8c) (Kruskal–Wallis, $p < 0.05$). At Lake Heideweiher measurements under ice in December 2018, showed 0.64 μM CH_4.

Lake Windsborn showed low seasonal variability in surface CH_4 concentrations. However, there were two distinct "peak moments" with increased surface CH_4 concentrations, in June/July 2017 and June 2018 (Figs 2, 3), reaching means of 2.9 and 6.6 μM, respectively (i.e., an increase by a factor of 1.93 and 4.4, respectively, compared to the mean). However, in general, similar CH_4 surface concentrations were measured over the entire Lake Windsborn, and no significant spatial differences were observed related to the water depth category (Kruskal–Wallis, $p < 0.05$). Under temporarily stratified conditions in August 2018, CH_4 accumulated in deep water up to 33 μM (Fig. S6). In March 2018, the CH_4 concentration at Lake Windsborn under the ice was 0.51 μM.

CH_4 emissions

Both lakes showed a clear seasonality in CH_4 emissions, with the highest fluxes in summer and subsequent decrease until November (Fig. 2). The overall mean flux weighted by area and time period for 2017 and 2018 was 3.7 ± 1.9 and 3.1 ± 0.8 mmol m^{-2} d^{-1} at Lake Windsborn and 19.6 ± 2.5 and 4.6 ± 0.4 mmol m^{-2} d^{-1} at Lake Heideweiher; the lakes did not significantly differ in terms of fluxes, but lake Heideweiher showed much more variability differences

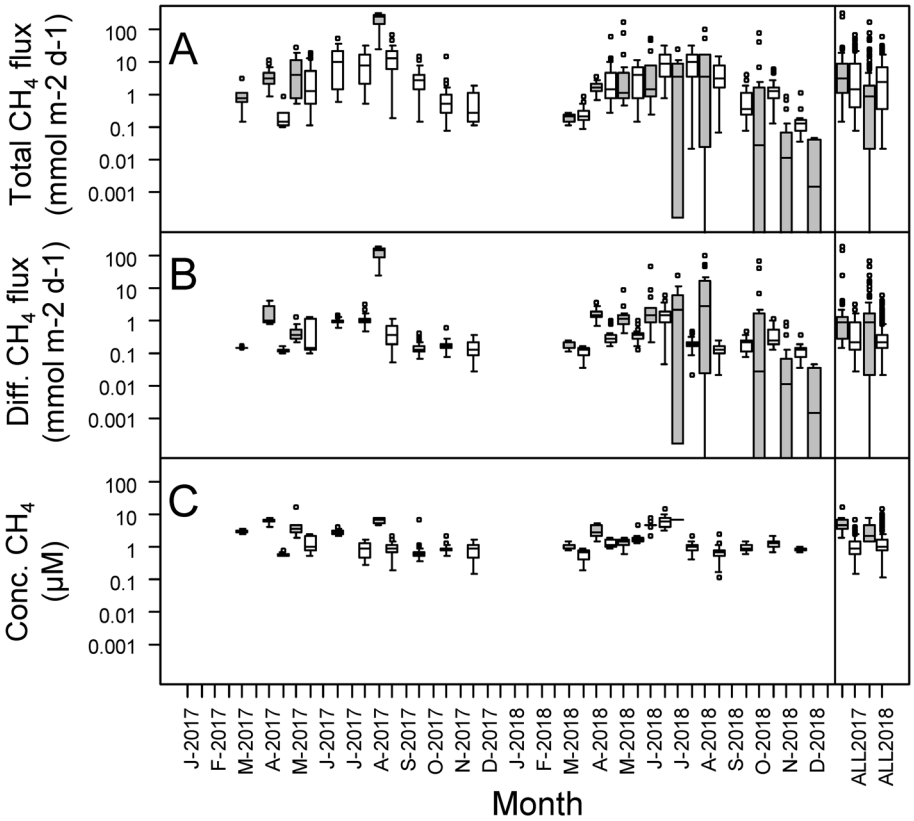

Fig. 2. Boxplot of total fluxes (**A**) (diffusive fluxes + ebullition), diffusive fluxes (**B**) and surface water concentrations (**C**) of CH_4 in Lake Heideweiher (gray boxplots) and Lake Windsborn (white boxplots) during 2017 and 2018. Between August 2018 and December 2018, Lake Heideweiher was completely dried up. Note the log10 scale on the *y*-axis. The boxes show 25 and 75 quartiles and the median; whiskers indicate data within 1.5 times of the interquartile range. Circles denote outliers.

between the years (Table 2). At Lake Heideweiher, the 2 years showed strong interannual differences. In summer 2017, the lake dried out only at the shore, and the center of the lake had a shallow water column of a maximum depth of 35 cm, the CH_4 emissions from the open water reached maxima as high as 205.1 ± 159.1 mmol $m^{-2}d^{-1}$, while emissions from the dry area decreased to 0.02 mmol m^{-2} d^{-1}, resulting in a whole lake mean flux of 138.4 mmol m^{-2} d^{-1}. Earlier in June 2018, only the shore areas dried out, also causing strong spatial variability of fluxes, with the highest fluxes of the year occurring from water-filled areas and the lowest fluxes from the dry areas. When Lake Heideweiher dried out completely in July 2018, the CH_4 fluxes decreased to a mean of 4.3 ± 9.9 mmol m^{-2} d^{-1} with a large spatial variability from restricted local wet spots. During the dry up, we even measured uptake of CH_4 up to −0.2 mmol m^{-2} d^{-1}. Regarding the water column depth categories, the total fluxes were significantly higher in the depth category of 100 compared to the depth categories of 50 and 75 (Kruskal–Wallis, $p < 0.05$) (Fig. S8). Only 4% of the total CH_4 flux was emitted from the shore areas (~ 50 cm) at Lake Heideweiher (Fig. 4; Table 3) while this depth category contributed an area proportion of 34%. Ebullition was observed from all depth categories, but the amount of bubbles and, thus, the total flux increased toward the center of both lake and with increasing water depth category (Table 3). The share of the ebullition in total fluxes was 65% in 2017 and 37% in 2018 (Table 2) but with high temporal variability. The diffusive fluxes showed no clear temporal trend; however, during dry periods the fluxes decreased strongly.

Lake Windsborn showed a clear seasonality with the highest CH_4 fluxes in summer (June–August) during both years (Fig. 2). Like the water column CH_4 concentrations, the diffusive fluxes also showed little variability and no significant differences between depth categories (Kruskal–Wallis, $p < 0.05$). By contrast, ebullition increased with increasing depth: Particularly, transect 3 showed lower ebullition and lower fluxes at the shore (Fig. 4). At the shore, 80% of the total flux was emitted by ebullition, whereas in the depth category 150 as much as 96% of the flux was from ebullition (Table 3).

Moreover, we observed that ebullition occurred earlier in the year in the central area. By midsummer, the differences between the sites were lower, and in fall ebullition was again higher in the central area. While in fall of 2017 ebullition abruptly decreased with concomitantly intensified

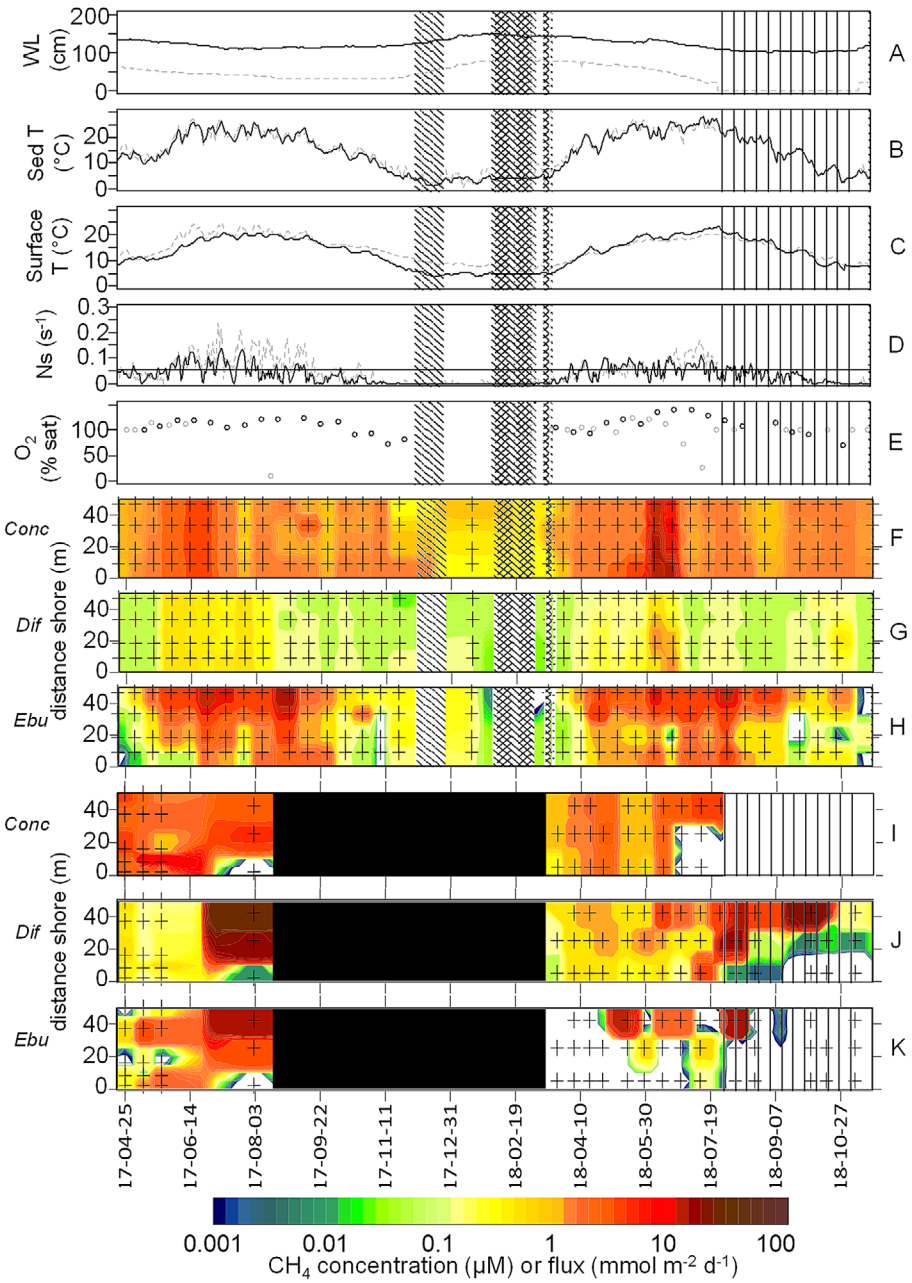

Fig. 3. Seasonal variability of the environmental factors of Lake Windsborn (black, solid line) and Lake Heideweiher (gray, dashed line) (**A**–**E**): Water level (**A**), surface water temperature (**B**), sediment temperature (**C**), Brunt–Väisälä stability frequency N_s (**D**), O_2 sat.—after the time point of drying up completely, we assumed 100% oxygen (**E**). Seasonal variability of CH_4 concentrations in water (**F**,**I**), diffusive fluxes (**G**,**J**), and ebullitive fluxes (**H**,**K**) in Lake Windsborn (**F**–**H**), and Lake Heideweiher (**I**–**K**) in relation to the distance to the shore. The mean of the transects for each depth category on each measurement day (crosses) provides the data basis for the IDW interpolation (inverse distance weighted). Black in panels **I**–**K** indicates missing data, and white indicates no detectable concentrations or fluxes. The diagonally left shaded area shows the ice cover at Lake Windsborn while the crossed area indicates the time when both lakes were ice covered. The vertical lines show the period of drying up at Lake Heideweiher.

mixing (Fig. 3D,H), in fall of 2018 the fluxes decreased first near the shore; with ongoing circulation of the water column, and the fluxes continued to decrease also elsewhere and reached their minimum in November, with almost zero fluxes, whereby the proportion of ebullition decreased from about 90–36%.

Relationships with environmental variables

Temperature

CH_4 fluxes were strongly correlated with temperature (Fig. 5). The fluxes increased exponentially with sediment temperature, following the Arrhenius function. The activation energies as obtained from the Arrhenius function were similar

Table 2. Annual whole-lake estimates of emissions in 2017 and 2018 using three different approaches and the relative annual amount of ebullition.

	Windsborn		Heideweiher	
	2017	2018	2017	2018
CH_4 annual flux (mmol m^{-2} d^{-1}) ± SE				
Mean of all measurements*	6.6 ± 0.8	5.7 ± 0.5	17.1 ± 7.1†	7.6 ± 0.4
Depth category proportion and day weighted‡	3.7 ± 1.9	3.1 ± 0.8	19.6 ± 2.5†	4.6 ± 0.4
Generalized linear model§	3.7 ± 0.2	4.6 ± 0.3	8.6 ± 0.5	4.2 ± 0.3
% ebullition‡	91	89	65	37

When calculating the mean of all measurements, no gap-filling data were used.
*Mean of chamber measurements in 2017 and 2018 without weighting.
†In 2017 there was a lack of data for the second half of the year at Lake Heideweiher. We filled this gap with the data of the water model (Table 4A). However, these estimates may be subject to larger errors.
‡Annual flux of 2017 and 2018 as the sum of individual fluxes weighted by proportion of the depth segment and linear interpolation between days of measurement. % Ebullition is based on this approach.
§Annual flux determined from the model's prediction. For the period and depth category with standing water column (waterlevel > 0 cm), the water model (Table 4A) was used whereas the dry model (Table 4B) was used for the time of drought of the respective category.

(~ 1.85 eV) in both lakes (Fig. 5A; Table S4). Temperature explained 43% of the total variance in fluxes. Neglecting spatial differences by using whole-lake daily means and considering only temporal patterns, sediment temperature could explain 72% (Heideweiher) and 82% (Windsborn) of the observed variance in fluxes over time.

Stratification and oxygen

The mostly daily but sometimes also several days long stratification in Lake Windsborn led to a reduction of the oxygen supply as long as the stratification continued and therefore represents a proxy for the oxygen concentration. Moreover, the stratification also induced a decoupling of the surface water from the underlying processes. The stability of stratification strongly intercorrelated with temperature, resulting in a high correlation with fluxes and was thus not included for modeling the flux.

In Lake Heideweiher, O_2 concentrations were closely related to CH_4 fluxes. When the water column was only a few centimeters, the oxygen pool in the water was rapidly consumed, and anoxic conditions adjusted (Fig. 3E). Under these conditions, we observed an enrichment of CH_4 in the surface water and an increase in the diffusive as well as in the ebullitive fluxes. The proportion of the diffusive flux therefore increased significantly. The first days of the dry period showed even higher emissions than the days immediately prior to dry period. (Fig. 5B).

Sediment organic matter quality

The sediment organic matter quality—expressed by C content and C : N ratio—explained 13% and 2% of the variability in CH_4 fluxes, respectively (Table 4A). The C content and the C : N ratio increased with water depth or distance to the shore in both lakes. Transect 3 of Lake Windsborn showed overall significantly lower C-contents, which corresponded with lower CH_4 emissions compared to the other transects (Fig. 5C). Thus, when considering only spatial differences through site-specific means, the C-content could explain 79.7% (Heideweiher) and 62% (Windsborn) of the variance in fluxes. Similarly, the C : N ratio could alone explain 50.1% (Heideweiher) and 40.5% (Windsborn) of the variance (Fig. 5D).

Drought phase

The onset of drying up in July 2018 changed the system at Lake Heideweiher in a way that other factors became important. Therefore, during the drought phase, the CH_4 fluxes were processed in a separate model. A depth category was considered dry when the water level at the respective chamber reached 0 cm. The depth category 50 dried up on 06 June 2018 and rewetted in the mid of March 2019, the category 75 dried up on 28 July 2018 and rewetted in the mid of January 2019 and the category 100 dried up on 07 August 2018 and rewetted in the beginning of December. The model, using only the $t_{drought}$ and the C-content (Table 4B), was able to explain about 84% of the variance of fluxes. $t_{drought}$ alone accounted for 76% of the variance (Table 4B). After a dry period of 30–50 d, the measured fluxes had declined to about 1% of the fluxes from open water areas before dry period. Just as in 2017, emissions increased significantly with decreasing water level and remained high for the first days of drought.

Discussion

Our study highlights the importance of spatiotemporal variability of CH_4 fluxes in temperate shallow lakes, as already reported for boreal systems (Natchimuthu et al. 2016). From our almost 2-year data set of biweekly sampling campaigns, results suggested that both lakes were strong sources of CH_4. The mean CH_4 fluxes for Lake Windsborn and Lake

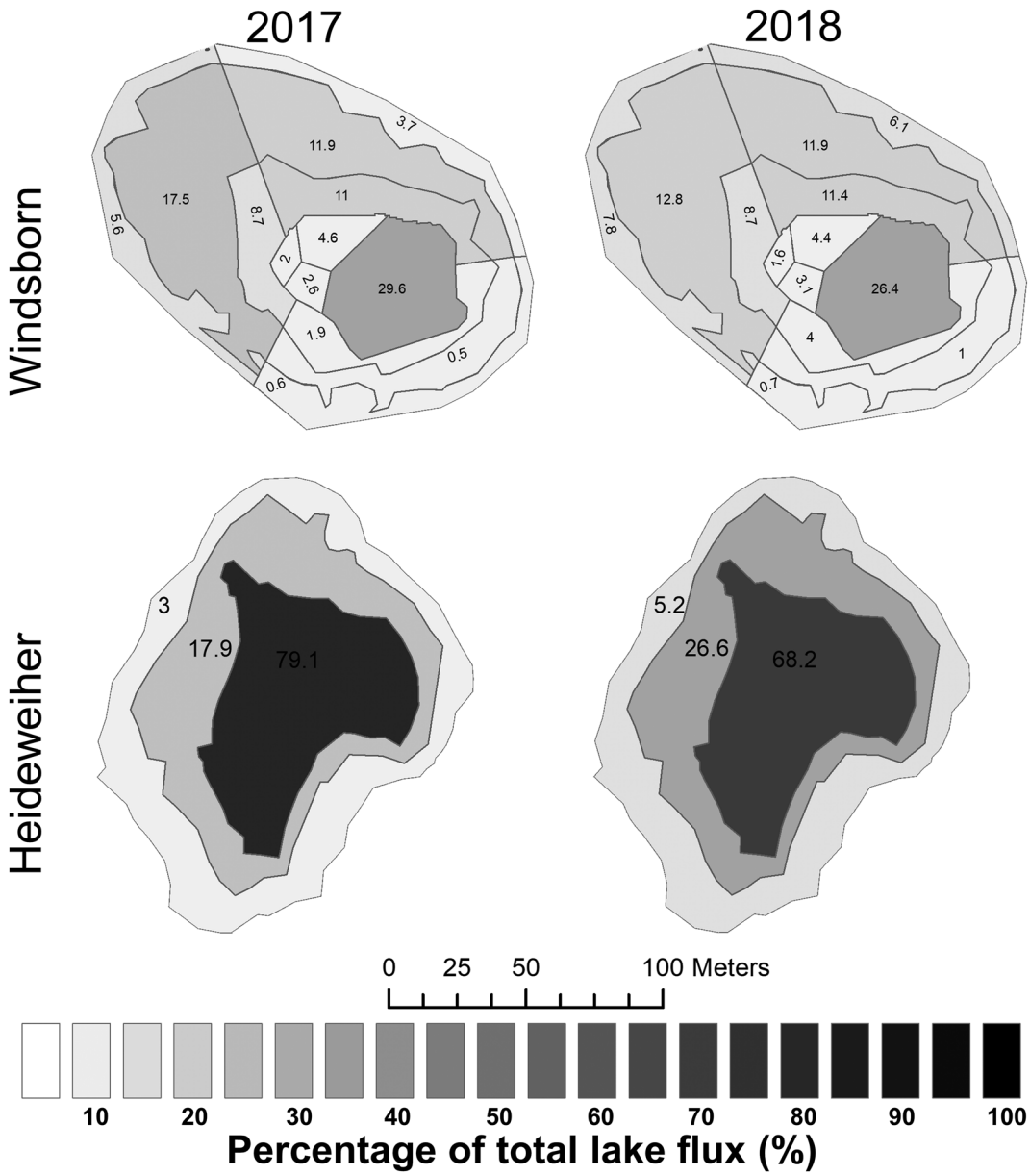

Fig. 4. The percentage of total flux from the different depth categories and transects according to Thiessen polygons. About 38.8%/35.5% (Windsborn) and 79.1%/68.2% (Heideweiher) of the total flux were from the depth category at the center of the lake. Note that the maximum depth of Lake Windsborn and Lake Heideweiher was 150 and 100 cm, respectively.

Heideweiher for both years in this study were 3.5 ± 20.5 and 12.2 ± 45.6 mmol m^{-2} d^{-1}, respectively, which was 12.5 and 43.6 times higher than mean emissions of similarly sized lakes (~ 1 ha) as reported elsewhere (Holgerson and Raymond 2016). In the review of Bastviken et al. (2011), average emissions of lakes between 25° and 54° latitude were 4.1 mmol m^{-2} d^{-1}. Our emissions measured at Lake Windsborn fell in a similar range (1.15 times lower), but the emissions measured at Lake Heideweiher exceeded this average by a factor of 2.98.

Lake Heideweiher can be described as rather productive, keeping in mind its water lily vegetation coverage and thus large input of organic material. Lake Windsborn is subject to a strong input of terrestrial material and is therefore more productive presumably contributing substrates to CH_4 formation. Hence, fluxes of both lakes are comparable with more productive lakes such as a eutrophic urban lake in the Netherlands with 14 mmol m^{-2} d^{-1} (van Bergen et al. 2019), or from or a hypertrophic Lake Priest Pot, Cumbria, England with 5 mmol m^{-2} d^{-1} (Casper et al. 2000). However, our data may not be directly comparable with data of previous studies reflecting considerably shorter time periods.

Table 3. Percentages of area and CH_4 emissions, and the percentage of ebullition of the respective total flux per depth type based on day-weighted data from the different depth categories within Lake Windsborn (WB) and Lake Heideweiher (HW), highlighting the hotspots of the CH_4 emissions.

	Percent of area		Percent of total flux		Percent of ebullition flux per depth type	
Depth type	WB	HW	WB	HW	WB	HW
50	21	34	12	3	81	56
75	n/a*	34	n/a*	20	n/a*	32
100	44	32	28	77	82	67
125	18	0	23	n/a*	93	n/a*
150	17	0	37	n/a*	97	n/a*

*In Lake WB, the depth category 75 was not considered seperately but included in depth category 100. In Lake HW, the depth categories 125 and 150 were not applicable (lake depth < 100 cm).

In contrast, Paul Lake in the United States, similar in size but poorer in nutrients and dissolved organic carbon (DOC), emitted only 1.51 mmol m^{-2} d^{-1} (Bastviken et al. 2008). The subtropical shallow freshwater Cattai wetland in Australia may have a comparable setting as Lake Heideweiher, especially due to similar geology (sand), environment (agriculture), drying-out period in summer and occurrence of water lilies (Jeffrey et al. 2019). The CH_4 emissions reported for this lake, amounting to 31.4 mmol m^{-2} d^{-1} (only open water flux), were considerably higher than the fluxes observed in our study in 2018 (4.8 mmol m^{-2} d^{-1}), but considering the on average 10°C warmer winters and 7°C warmer summers in Australia, this may be explained by temperature. Natchimuthu et al. (2014) also reported high summer CH_4 fluxes of 8.0 mmol m^{-2} d^{-1} from a shallow pond in Sweden and concluded that any shallow lake or pond can emit fluxes as from tropical systems during warm periods, given similar productivity. Our study also showed high emissions during particular warm periods and also throughout the year, with a high fraction of ebullition of around 90% for Lake Windsborn and 40% for Lake Heideweiher, respectively. This range is consistent with the overall reported high proportion of ebullition of about 50% to > 90% for comparable lakes (Bastviken et al. 2011; Natchimuthu et al. 2016; van Bergen et al. 2019). Ebullition thus must be considered to representatively estimate whole-lake CH_4 fluxes, particularly in shallow lakes. As confirmed by our study, the spatial–temporal variability also needs to be considered in the integration of the fluxes.

Spatial variability of CH_4 fluxes in relation to environmental drivers.

Sediment organic matter

The spatial differences were influenced by the quantity and quality of the deposited sediment as also suggested elsewhere (e.g., Maeck et al. 2013). As sediment quality changes much more slowly than the metrological parameters, sediment properties set the spatial framework upon which factors influencing temporal variability may act (Fig. 4, Table 4). Regarding spatial variability, we observed an increase in CH_4 emissions from the shore towards the center, just as the sediment C-content increased towards the center of the lakes. These results supported our hypothesis that the input of organic matter can explain the within-lake spatial differences. This may seem contradictory to numerous previous studies, in which the highest fluxes were typically observed in littoral areas (Bastviken et al. 2004; Hofmann 2013; DelSontro et al. 2016; Natchimuthu et al. 2016). However, the investigated lakes in this study are overall shallow, not exceeding a depth of 100 cm (Heideweiher) or 200 cm (Windsborn), and, thus, they may not develop characteristics of distinct pelagic or a littoral zone—the littoral zone may rather cover the whole lakes. Van de Bogert et al. (2012) and Kankaala et al. (2013) both concluded that it is not the distance to shoreline that is important but rather other factors, such as microbial decomposition of allochthonous or littoral organic matter, which can be, but is not necessarily related to the distance to the shore. While the distance to shore may not be a relevant flux predictor in the studied lakes, we noted a relationship between sediment C-content and C : N ratio and total CH_4 emissions that could explain a large part of the within-lake spatial variability (Fig. 5).

According to a recent study on sediment properties in Lake Windsborn (Praetzel et al. 2020), the higher C : N ratios toward the shore in Lake Windsborn indicate an input of allochthonous (terrestrial) material near the shore and sedimentation of autochthonous (aquatic) organic matter in the lake center. It is known that allochthonous material is more difficult to decompose than material of autochthonous origin (Sobek et al. 2012; Grasset et al. 2018). This may explain the lower CH_4 emissions in the near-shore areas. This would further explain the negative correlation between CH_4 emissions and the C : N ratio, as allochthonous material is typically higher in C : N ratio (Meyers 1994).

In Lake Heideweiher, a strong mineralization during the drying period is also reflected in the spatial differences in the C-content. The littoral area that may fall dry for several

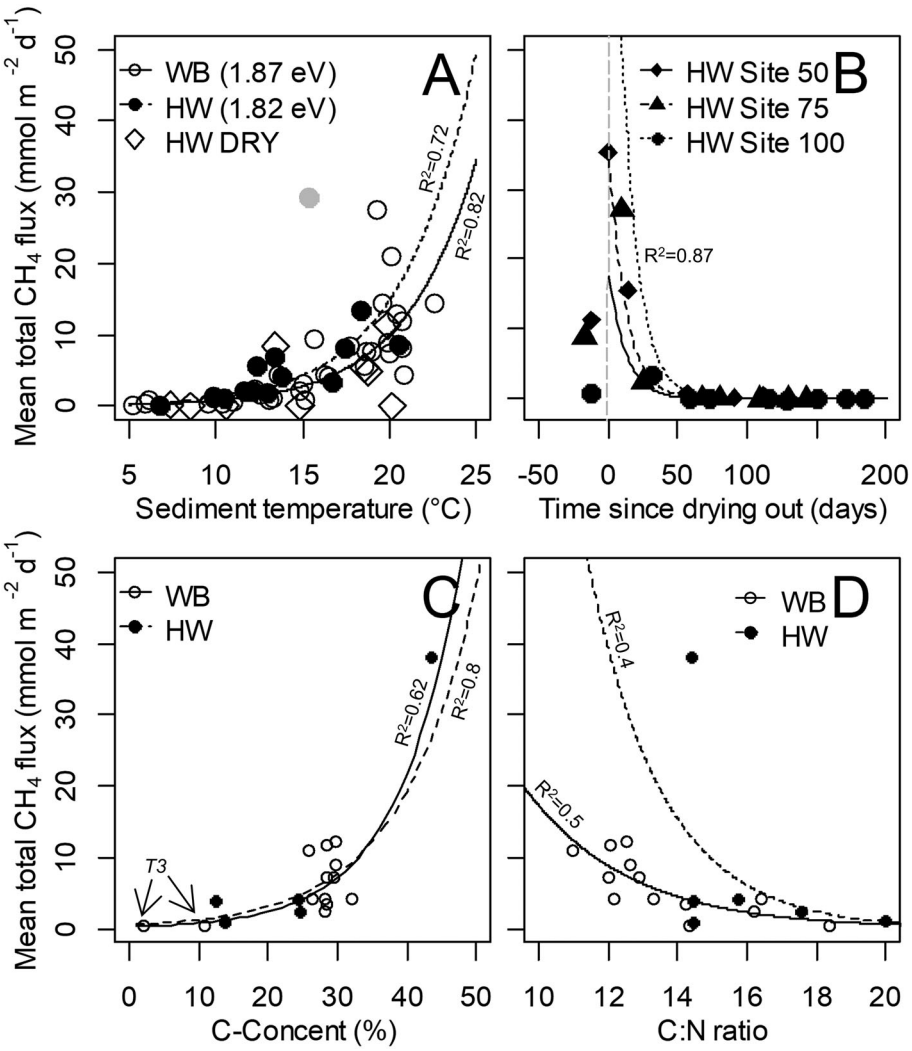

Fig. 5. Relationships between sediment temperature (**A**) and daily mean total CH_4 flux at Lake Windsborn (WB—open circles and solid line) and Lake Heideweiher (HW—black dots and dashed line). The data at the time of drying out (diamonds) were separated and are not included in the model, also the outlier (gray point) was not considered (for details of the model see Table S4). Relationships between time since drying out and daily mean total CH_4 flux (**B**). As the different depth categories had dried up at different times, zero was assumed to be the point in time when the respective depth category was dry (gray dashed line). The site 50 was already dry on the 9th of June 2017, the site 75 was dry on the 21st of July 2018 and the site 100 was dry on the 8th of August 2018. Until the end of the year 2018 only site 100 was covered with water again after ~ 120 d. Lines show the fitted general linear model for dry conditions (Table 4B). Relationships between organic matter quality parameter C-content in the sediment (**C**) with marked sites 50 and 100 of transect 3 of Lake Windsborn (T3), C : N ratio (**D**) and site-specific mean values mean total CH_4 flux (for details of the model see Table S4).

months every year, was significantly lower in C-content, about 13% of C by weight, compared to the center of the lake, which contained about 43%. As a result of drying up and increased aerobic respiration, likely a high loss of C occurred. In addition, due to the occurrence of macrophytes (water lilies), a large amount of macrophyte litter entered the system. This may contribute to the high difference in C content between sites and in the center of the lake, a higher cover of water lilies likely increased the input of litter, fueling methanogenesis, as reported by Kankaala et al. (2003).

A major source of uncertainty that needs to be addressed in future studies is the cover by floating macrophytes, which we did not include in this study. In addition to (1) local sediment accumulation leading to increased gas production, interactions between (2) plant roots and the sediment due to plant movement or (3) gas conduction through aerenchyma (affecting both plant mediated CH_4 emission and O_2 intrusion in sediments hampering sediment CH_4 production and stimulating CH_4 oxidation) can lead to plant effects on CH_4 emissions during the growing season (May–October) (Jeffrey et al. 2019; Villa et al. 2020). Furthermore, plants with floating leaves or

Table 4. Generalized linear model for predicting Total CH_4 flux (mmol m^{-2} d^{-1}) during water filled phase (A) and during drought (B). Estimates are given as natural logaritm (ln). All contained covariates were tested for significance.

Model water (A)	Unit	Estimate	SE	*p* Value	R^2
Sediment T (SedT)	°C	0.23	0.01	< 0.01	0.45
C-content in sediment (C)	%	0.07	0.006	< 0.01	0.13
C : N	Ratio	−0.11	0.03	< 0.01	0.02
(Intercept)		−2.71	0.46	—	—
$\ln(Flux_{water}) = -2.71 + 0.23 \cdot SedT + 0.07 \cdot C - 0.11 \cdot C : N$					0.60
Model drought (B)	**Unit**	**Estimate**	**SE**	***p* Value**	R^2
Time since drought ($t_{drought}$)	Days	−0.08	0.009	< 0.01	0.76
C-content (C)	%	0.06	0.03	< 0.05	0.08
(Intercept)		2.03	0.97	—	—
$\ln(Flux_{dry}) = 2.03 - 0.08 t_{drought} + 0.06 \cdot C$					0.84

being emergent can affect gas exchange by influencing *k* and the contact area between water and the atmosphere (Jeffrey et al. 2019). Consequently, plant can influence CH_4 fluxes in complex ways that deserve further attention.

Temporal variability of CH_4 fluxes and underlying controls

Effects of temperature

Besides spatial differences, also seasonal factors influenced CH_4 fluxes. Conforming our hypothesis, the CH_4 fluxes followed the seasonal temperature amplitude resulting in the highest fluxes in the summer months. Temperature, especially sediment temperature more than surface water temperature, best explained the emissions of CH_4, confirming previous studies and the temperature sensitivity of ebullition (Duc et al. 2010; Yvon-Durocher et al. 2014; DelSontro et al. 2016; Natchimuthu et al. 2016; Aben et al. 2017; Jansen et al. 2019; Jeffrey et al. 2019; van Bergen et al. 2019). The fluxes showed an exponential increase with temperature, following the Arrhenius equation. Temperature is known to act as a major control on all microbially mediated processes, including overall respiration and CH_4 formation (van Hulzen et al. 1999). However, temperature was reported to have a weaker effect on CH_4 oxidation than on formation, so that at higher temperatures total emissions are expected to increase (Duc et al. 2010).

The determined activation energy of net CH_4 formation in this study (derived from temperature response of CH_4 emission) of ~ 1.85 eV is higher than average values from available studies (0.96 eV), but is still within the upper end of the reported range (Yvon-Durocher et al. 2014). Shallow lakes may thus be particularly sensitive to temperature changes due to a large amount of easily decomposable material within a comparably small water body.

Stratification and O_2 content

Most parts of the lakes were vertically and horizontally partially mixed at least during the night, which resulted in well oxygenated water body at 72% of the time in both lakes creating potential for CH_4 oxidation (MacIntyre and Melack 1995; Bastviken et al. 2002). Consequently, CH_4 concentrations were relatively stable and in dynamic equilibrium between the oxidation and the CH_4 diffusively emitted by the sediment and the diffusive fluxes to the atmosphere. Thus, the CH_4 concentration was largely decoupled from the seasonal temperature amplitude. This contradicted our hypothesis that a higher temperature would result in higher production and higher diffusive sediment fluxes and thus higher CH_4 surface water concentrations, and indicate that diffusive flux is not always sensitive to temperature. However, the oxygen concentrations under stratified conditions dropped sharply, indicating periods without complete nighttime mixing (Fig. S7). This was accompanied by an enrichment of CH_4 in the water in the larger water body of Lake Windsborn. Due to mostly daily mixing, however, no larger quantities could accumulate, thus this phenomenon was not relevant for total emission. Due to the high temperature and therefore low solubility of oxygen at Lake Heideweiher in summer 2017, and, due to the low water movement, oxygen pools could not be replenished at the rate O_2 was consumed, resulting in almost anoxic conditions even in the very shallow water body (maximal depth 35 cm) (Fig. 3). Under these conditions, diffusive CH_4 fluxes were substantial, likely due to the short distance between CH_4 forming sediments and the atmosphere. These extremely high emissions added more to the total yearly emissions than the reduction of the emissions due to the dried-out littoral areas in 2017. In 2018, the total emissions again increased until the lake completely dried out, and, although the dry areas emitted almost no CH_4, the water-saturated areas, covering only 30% of the total lake area, were so CH_4-rich that altogether more CH_4 was emitted from these areas in the dry summer than from the larger water-saturated area in spring. Short-term drought of only a few days would according to our data not reduce emissions strongly, as the sediment was still sufficiently saturated with water and anoxic, obviously maintaining methanogenic niches. The

increased emissions directly in the first days after drying can be explained by the emptying of the sediment reservoir or also by the strong heating of the open sediment. Only a longer drought resulted in complete oxidation of the sediment, inhibiting methanogenesis and promoting aerobic mineralization of the sediment organic carbon (Jeffrey et al. 2019; Marcé et al. 2019). Under such conditions, the remaining amount of emitted CH_4 depends on small-scale levels of moisture in the sediment and less on temperature and accordingly, CH_4 emissions did not show correlation with temperature under such conditions. Increased amounts of CH_4 were emitted during the onset of drought (compared to fluxes with existing water bodies), but after a drought period of 10–15 d, the drought resulted in strong reduction of CH_4 emission. Hence, the decreasing effect of drought on fluxes was not noticeable in the short term but only during a longer drought phase after the initially high fluxes declined.

The partial rewetting of Lake Heideweiher in December was also accompanied by the onset of an ice cover and it was not possible to continue flux measurements thereafter. However, it can be assumed that a delay in methanogenesis can be expected during rewetting, which depends on the intensity and duration of the drying out. This is explained by a regeneration of inorganic and organic electron acceptors during the oxidation of the sediment, which delay the onset of methanogenesis due to competitive, thermodynamic suppression (Knorr et al. 2008; Lau et al. 2015; Gao et al. 2019). Due to reported time scales of such suppression and due to low temperatures in winter, it can be assumed that after prolonged drought phases, production of CH_4 is likely completely inhibited for the subsequent winter months and perhaps parts of the spring. Altogether, water dry out did not have an immediate short-term effect on the annual CH_4 balance, but may very well have a considerable delayed effect reaching into during the rewetting period.

In contrast to previous studies with a high contribution of ice-out fluxes (Michmerhuizen et al. 1996; Karlsson et al. 2013), we did not observe a large ice-out flux. During the ice cover, CH_4 did not accumulate, leveling off at 0.51 μM (Windsborn) and 0.64 μM (Heideweiher) and thus below the annual mean (Fig. S3). According to the study of Jansen et al. (2020), gas storage increases with the length of the ice cover season due to ongoing production from the sediment. The relatively short ice cover and permanent availability of O_2 and inorganic and organic electron acceptors in combination with the low temperature likely prevented CH_4 accumulation.

Conclusions

The temperate shallow lakes investigated in this study emitted high amounts of CH_4 with both high spatial and temporal variabilities within and between the lakes. The depth–flux relationship with often found in deeper lakes was not apparent in these shallow lakes and instead the spatial differences were explained by the amount of allochthonous C and the organic matter quality in terms of C : N ratio in the sediments. Temporal variability was best explained by a positive relationship between CH_4 emissions and temperature, corresponding to a higher temperature sensitivity than found for larger lakes. In addition to temperature, anoxic conditions increased CH_4 concentrations as a result of stratification. These findings have important implications when generalizing existing knowledge for the large number of small and shallow lakes. In these systems, a strong spatial variability of fluxes as driven by local differences in sediment properties is interacting with strong seasonal temperature effects, potentially amplifying these differences. Morevoer, a drying-up period showed progressively higher emissions as the water level decreased, followed by decreasing emissions as sediments were exposed to the air. Hence, drought periods in productive, shallow lakes can on the one hand reduce annual emissions, but boost emissions from warm and shallow wet areas during the drought phase. We were able to show that for whole lake emissions estimates, short-term and small-scale measurements are insufficient for addressing the high variability of fluxes. Under climate change with expected higher temperatures and drier summers in the temperate zone, more systematic sampling is needed to provide accurate estimates of greenhouse gas emissions from small lakes, and large interannual variability can be expected depending on temperature and the intensities of drought.

References

Aben Ralf C. H., and others. 2017. Cross continental increase in methane ebullition under climate change. Nature Communications **8**. doi:10.1038/s41467-017-01535-y

Bastviken, D., J. Ejlertsson, and L. Tranvik. 2002. Measurement of methane oxidation in lakes: A comparison of methods. Environ. Sci. Technol. **36**: 3354–3361. doi:10.1021/es010311p

Bastviken, D., J. J. Cole, M. L. Pace, and L. J. Tranvik. 2004. Methane emissions from lakes: Dependence of lake characteristics, two regional assessments, and a global estimate. Global Biogeochem. Cycl. **18**: GB4009. doi:10.1029/2004GB002238

Bastviken, D., J. J. Cole, M. L. Pace, and M. C. van de Bogert. 2008. Fates of methane from different lake habitats: Connecting whole-lake budgets and CH_4 emissions. J. Geophys. Res. **113**: G02024. doi:10.1029/2007JG000608

Bastviken, D., L. J. Tranvik, J. A. Downing, P. M. Crill, and A. Enrich-Prast. 2011. Freshwater methane emissions offset the continental carbon sink. Science **331**: 50. doi:10.1126/science.1196808

Casper, P., S. C. Maberly, G. H. Hall, and B. J. Finlay. 2000. Fluxes of methane and carbon dioxide from a small productive lake to the atmosphere. Biogeochemistry **49**: 1–19. doi:10.1023/A:1006269900174

Chen Chen-Tung A., and Millero Frank J. 1986. thermodynamic properties for natural waters covering only the limnological range1. Limnology and Oceanography **31**: 657–662. doi:10.4319/lo.1986.31.3.0657

DelSontro, T., L. Boutet, A. St-Pierre, P. A. del Giorgio, and Y. T. Prairie. 2016. Methane ebullition and diffusion from northern ponds and lakes regulated by the interaction between temperature and system productivity. Limnol. Oceanogr. **61**: S62–S77. doi:10.1002/lno.10335

Downing, J. A. 2010. Emerging global role of small lakes and ponds: Little things mean a lot. Limnetica **29**: 9–24. doi:10.23818/limn.29.02

Duc, N. T., P. Crill, and D. Bastviken. 2010. Implications of temperature and sediment characteristics on methane formation and oxidation in lake sediments. Biogeochemistry **100**: 185–196. doi:10.1007/s10533-010-9415-8

Dunn, O. J. 1964. Multiple Comparisons Using Rank Sums. Technometrics **6**: 241–252.

Gålfalk, M., D. Bastviken, S. Fredriksson, and L. Arneborg. 2013. Determination of the piston velocity for water–air interfaces using flux chambers, acoustic Doppler velocimetry, and IR imaging of the water surface. Eur. J. Vasc. Endovasc. Surg. **118**: 770–782. doi:10.1002/jgrg.20064

Gao, C., M. Sander, S. Agethen, and K.-H. Knorr. 2019. Electron accepting capacity of dissolved and particulate organic matter control CO_2 and CH_4 formation in peat soils. Geochim. Cosmochim. Acta **245**: 266–277. doi:10.1016/j.gca.2018.11.004

Grasset, C., R. Mendonça, G. Villamor Saucedo, D. Bastviken, F. Roland, and S. Sobek. 2018. Large but variable methane production in anoxic freshwater sediment upon addition of allochthonous and autochthonous organic matter. Limnol. Oceanogr. **63**: 1488–1501. doi:10.1002/lno.10786

Gray, E., E. B. Mackay, J. A. Elliott, A. M. Folkard, and I. D. Jones. 2020. Wide-spread inconsistency in estimation of lake mixed depth impacts interpretation of limnological processes. Water Res. **168**: 115136. doi:10.1016/j.watres.2019.115136

Hofmann, H. 2013. Spatiotemporal distribution patterns of dissolved methane in lakes: How accurate are the current estimations of the diffusive flux path? Geophys. Res. Lett. **40**: 2779–2784. doi:10.1002/grl.50453

Holgerson, M. A., and P. A. Raymond. 2016. Large contribution to inland water CO_2 and CH_4 emissions from very small ponds. Nat. Geosci. **9**: 222–226. doi:10.1007/s10533-015-0099-y

Huotari J., and others. 2011. Long-term direct CO2flux measurements over a boreal lake: Five years of eddy covariance data. Geophysical Research Letters **38**. doi:10.1029/2011gl048753

IPCC. 2013. Climate change 2013. *In* T. F. Stocker et al. [eds.], The physical science basis. Contribution of Working Group I to the Fifth Assessment Report of the Intergovernmental Panel on Climate Change. Cambridge Univ. Press.

Jansen, J., B. F. Thornton, M. M. Jammet, M. Wik, A. Cortés, T. Friborg, S. MacIntyre, and P. M. Crill. 2019. Climate-sensitive controls on large spring emissions of CH_4 and CO_2 from Northern Lakes. Eur. J. Vasc. Endovasc. Surg. **124**: 2379–2399. doi:10.1029/2019JG005094

Jansen, J., B. F. Thornton, A. Cortés, J. Snöälv, M. Wik, S. MacIntyre, and P. M. Crill. 2020. Drivers of diffusive CH_4 emissions from shallow subarctic lakes on daily to multi-year timescales. Biogeosciences **17**: 1911–1932. doi:10.5194/bg-17-1911-2020

Jeffrey, L. C., D. T. Maher, S. G. Johnston, B. P. Kelaher, A. Steven, and D. R. Tait. 2019. Wetland methane emissions dominated by plant-mediated fluxes. Contrasting emissions pathways and seasons within a shallow freshwater subtropical wetland. Limnol. Oceanogr. **64**: 1895–1912. doi:10.1002/lno.11158

Kankaala, P., T. Käki, and A. Ojala. 2003. Quality of detritus impacts on spatial variation of methane emissions from littoral sediment of a boreal lake. Arch.Hydrobiol. **157**: 47–66. doi:10.1127/0003-9136/2003/0157-0047

Kankaala, P., J. Huotari, T. Tulonen, and A. Ojala. 2013. Lake-size dependent physical forcing drives carbon dioxide and methane effluxes from lakes in a boreal landscape. Limnol. Oceanogr. **58**: 1915–1930. doi:10.4319/lo.2013.58.6.1915

Karlsson, J., R. Giesler, J. Persson, and E. Lundin. 2013. High emission of carbon dioxide and methane during ice thaw in high latitude lakes. Geophys. Res. Lett. **40**: 1123–1127. doi:10.1002/grl.50152

Knorr, K.-H., B. Glaser, and C. Blodau. 2008. Fluxes and ^{13}C isotopic composition of dissolved carbon and pathways of methanogenesis in a fen soil exposed to experimental drought. Biogeosciences **5**: 1457–1473. doi:10.5194/bg-5-1457-2008

Lau, M. P., M. Sander, J. Gelbrecht, and M. Hupfer. 2015. Solid phases as important electron acceptors in freshwater organic sediments. Biogeochemistry **123**: 49–61. doi:10.1007/s10533-014-0052-5

MacIntyre, S., and J. M. Melack. 1995. Vertical and horizontal transport in lakes: Linking littoral, benthic, and pelagic habitats. J. North Am. Benthol. Soc. **14**: 599–615. doi:10.2307/1467544

Maeck, A., T. DelSontro, D. F. McGinnis, H. Fischer, S. Flury, M. Schmidt, P. Fietzek, and A. Lorke. 2013. Sediment trapping by dams creates methane emission hot spots. Environ. Sci. Technol. **47**: 8130–8137. doi:10.1021/es4003907

Marcé, R., B. Obrador, L. Gómez-Gener, N. Catalán, M. Koschorreck, M. I. Arce, G. Singer, and D. von Schiller. 2019. Emissions from dry inland waters are a blind spot in the global carbon cycle. Earth-Sci. Rev. **188**: 240–248. doi:10.1016/j.earscirev.2018.11.012

Mattson, M. D., and G. E. Likens. 1990. Air pressure and methane fluxes. Nature **347**: 718–719. doi:10.1038/347718b0

Meyers, P. A. 1994. Preservation of elemental and isotopic source identification of sedimentary organic matter. Chem. Geol. **114**: 289–302. doi:10.1016/0009-2541(94)90059-0

Michmerhuizen, C. M., R. G. Striegl, and M. E. McDonald. 1996. Potential methane emission from north-temperate lakes following ice melt. Limnol. Oceanogr. **41**: 985–991. doi:10.4319/lo.1996.41.5.0985

Natchimuthu, S., B. P. Selvam, and D. Bastviken. 2014. Influence of weather variables on methane and carbon dioxide flux from a shallow pond. Biogeochemistry **119**: 403–413. doi:10.1007/s10533-014-9976-z

Natchimuthu, S., I. Sundgren, M. Gålfalk, L. Klemedtsson, P. Crill, Å. Danielsson, and D. Bastviken. 2016. Spatio-temporal variability of lake CH_4 fluxes and its influence on annual whole lake emission estimates. Limnol. Oceanogr. **61**: S13–S26. doi:10.1002/lno.10222

Praetzel, L. S. E., N. Plenter, S. Schilling, M. Schmiedeskamp, G. Broll, and K.-H. Knorr. 2020. Organic matter and sediment properties determine in-lake variability of sediment CO_2 and CH_4 production and emissions of a small and shallow lake. Biogeosciences **17**: 5057–5078. doi:10.5194/bg-17-5057-2020

R Core Team. 2018. R: A language and environment for statistical computing. Vienna, Austria: R Foundation for Statistical Computing.

Sander, R. 1999. Compilation of Henry's law constants for inorganic and organic species of potential importance in environmental chemistry. Max-Planck Institute of Chemistry.

Saunois, M., and others. 2020. The global methane budget 2000–2017. Earth Syst. Sci. Data **12**: 1561–1623. doi:10.5194/essd-12-1561-2020

Schilder, J., D. Bastviken, M. Hardenbroek, P. Kankaala, P. Rinta, T. Stötter, and O. Heiri. 2013. Spatial heterogeneity and lake morphology affect diffusive greenhouse gas emission estimates of lakes. Geophys. Res. Lett. **40**: 5752–5756. doi:10.1002/2013GL057669

Sobek, S., T. DelSontro, N. Wongfun, and B. Wehrli. 2012. Extreme organic carbon burial fuels intense methane bubbling in a temperate reservoir. Geophys. Res. Lett. **39**: L01401. doi:10.1029/2011GL050144

Tranvik, L. J., and others. 2009. Lakes and reservoirs as regulators of carbon cycling and climate. Limnol. Oceanogr. **54**: 2298–2314. doi:10.4319/lo.2009.54.6_part_2.2298

van Bergen, T. J. H. M., and others. 2019. Seasonal and diel variation in greenhouse gas emissions from an urban pond and its major drivers. Limnol. Oceanogr. **64**: 2129–2139. doi:10.1002/lno.11173

van de Bogert, M. C., D. L. Bade, S. R. Carpenter, J. J. Cole, M. L. Pace, P. C. Hanson, and O. C. Langman. 2012. Spatial heterogeneity strongly affects estimates of ecosystem metabolism in two north temperate lakes. Limnol. Oceanogr. **57**: 1689–1700. doi:10.4319/lo.2012.57.6.1689

van Hulzen, J. B., R. Segers, P. M. van Bodegom, and P. A. Leffelaar. 1999. Temperature effects on soil methane production: An explanation for observed variability. Soil Biol. Biochem. **31**: 1919–1929. doi:10.1016/S0038-0717(99)00109-1

Verpoorter, C., T. Kutser, D. A. Seekell, and L. J. Tranvik. 2014. A global inventory of lakes based on high-resolution satellite imagery. Geophys. Res. Lett. **41**: 6396–6402. doi:10.1002/2014GL060641

Villa, J. A., Y. Ju, T. Stephen, C. Rey-Sanchez, K. C. Wrighton, and G. Bohrer. 2020. Plant-mediated methane transport in emergent and floating-leaved species of a temperate freshwater mineral-soil wetland. Limnol. Oceanogr. **65**: 1635–1650. doi:10.1002/lno.11467

Weinert, M., D. Remy, and E. P. Löhnert. 2000. Hydrogeologische systemanalyse des naturschutzgebietes. Abh. Westf. Mus. Naturk. **62**: 41–172.

Wik, M., and others. 2018. Sediment characteristics and methane ebullition in three subarctic lakes. Eur. J. Vasc. Endovasc. Surg. **123**: 2399–2411. doi:10.1029/2017JG004298

Yvon-Durocher, G., A. P. Allen, D. Bastviken, R. Conrad, C. Gudasz, A. St-Pierre, N. Thanh-Duc, and P. A. del Giorgio. 2014. Methane fluxes show consistent temperature dependence across microbial to ecosystem scales. Nature **507**: 488–491. doi:10.1038/nature13164

Acknowledgments

This study was funded by the Deutsche Forschungsgemeinschaft (German Research Foundation, DFG; grant No. BL563/25-1). DB contributions were funded by the European Research Council (ERC) under the European Union's Horizon 2020 research and innovation programme (grant agreement No. 725546). We thank Rebecca Pabst, Jasmin Gesing, George Wittenbrink and Andreas Malkus for their support in the field. We thank the laboratory technicians of the laboratory of the Institute of Landscape Ecology as well as the student assistants for their assistance during laboratory work. This paper is dedicated to the memory of Christian Blodau, who initiated the project until he tragically passed away in July 2016. We thank two anonymous reviewers for their thoughtful comments that helped to improve this paper.

Conflict of Interest

None declared.

Submitted 28 February 2020
Revised 05 October 2020
Accepted 01 March 2021

Associate editor: John Downing